Coastal Engineering 83 (2014) 15–23

Contents lists available at ScienceDirect

Coastal Engineering

journal homepage: www.elsevier.com/locate/coastaleng

Distribution of individual wave overtopping volumes in shallow water wave conditions

Jørgen Quvang Harck Nørgaard *, Thomas Lykke Andersen, Hans F. Burcharth

Department of Civil Engineering, Aalborg University, Sohngaardsholmsvej 57, DK-9000, Denmark

ARTICLE INFO

Article history:
Received 15 November 2012
Received in revised form 27 August 2013
Accepted 18 September 2013
Available online 16 October 2013

Keywords:
Rubble-mound breakwater
Wave overtopping
Individual overtopping volumes
Maximum overtopping volume
Physical modeling
Wave height distribution

ABSTRACT

This paper contributes to a better knowledge on the distribution of individual wave overtopping volumes in shallow-water wave conditions. Results from new two-dimensional physical model tests on typical rubble-mound breakwater geometries indicate that the formulae by Besley (1999) are underestimating the number of individual overtopping waves in non-Rayleigh-distributed, shallow-water wave conditions. Additionally, the proposed shape factors by Franco et al. (1994), Van der Meer and Janssen (1994), Victor et al. (2012) in the two-parameter Weibull-distribution, which is normally used for describing individual wave overtopping volumes, have been seen to over predict the largest overtopping volumes in depth-limited waves. Correction terms based on the incident wave height distributions are introduced in the present paper to modify the existing formulations by Besley (1999), Franco et al. (1994), Van der Meer and Janssen (1994), and Victor et al. (2012). The modifications significantly improve the predictions of the largest overtopping volumes in shallow-water wave conditions.

1. Introduction

Wave overtopping can affect buildings, persons etc. located behind a sea defence structure and is usually specified as a design parameter with a specific return period. Normally, the average wave overtopping rate, q, is used as a design parameter. However, in recent time Franco et al. (1994) suggested instead to use the individual wave overtopping volumes as design criteria, such as the maximum individual wave overtopping volume during a design storm, V_{max}, since this is believed to provide a better design measure than the average overtopping rate. The reason is that the largest overtopping volumes during the storm will most likely cause the damages to buildings etc. in the hinterland. The EurOtop manual by Pullen et al. (2007) provided tolerable individual wave overtopping levels.

Several researchers have suggested probability distribution functions for individual wave overtopping volumes on coastal defence structures; Franco et al. (1994), Van der Meer and Janssen (1994), Besley (1999), Pullen et al. (2007), Lykke Andersen et al. (2009), and Victor et al. (2012). Many studies are, however, based on relatively deep-water wave conditions, and are believed to provide conservative predictions of the largest individual wave overtopping volumes in depth-limited conditions.

It should, however, be mentioned, that the depth-limitation effects have gained an increasing attention in recent time. As an example, Pullen et al. (2007) used the first negative moment of the energy spectrum, $T_{-1,0}$, in many of the design formulae instead of the commonly used peak period, T_p. The reason is that $T_{-1,0}$ is proportional to the wave energy flux and is thus more appropriate than T_p to introduce the effects of changes in the energy spectra in shallow water wave conditions, c.f. Van Gent (2001).

This paper presents a review of the state of art knowledge including an evaluation of the performance of existing formulations in depth-limited wave conditions by comparing them against new two-dimensional physical model tests in shallow-water wave conditions. Based on this, modifications are suggested to more effectively account for the effects of shallow-water wave conditions in existing distribution functions for individual overtopping wave volumes from previous studies.

2. Existing knowledge

The probability of wave overtopping is defined by (1) in which N_{ow} is the number of individual overtopping waves and N_w is the total number of waves.

$$P_{ow} = \frac{N_{ow}}{N_w} \tag{1}$$

The number of individual overtopping waves can be predicted from (2) given by Besley (1999) where T_m is the mean wave period in the time domain, H_s is the significant wave height in the time domain at the toe of the structure, and q is the average overtopping rate.

* Corresponding author at. Department of Civil Engineering, Aalborg University, Sohngaardsholmsvej 57, DK-9000, Denmark. Tel.: +4524846077.
E-mail addresses: jhn@civil.aau.dk (J.Q.H. Nørgaard), tla@civil.aau.dk (T. Lykke Andersen), hansburcharth@gmail.com (H.F. Burcharth).

0378-3839/$ – see front matter © 2013 Elsevier B.V. All rights reserved.
http://dx.doi.org/10.1016/j.coastaleng.2013.09.003

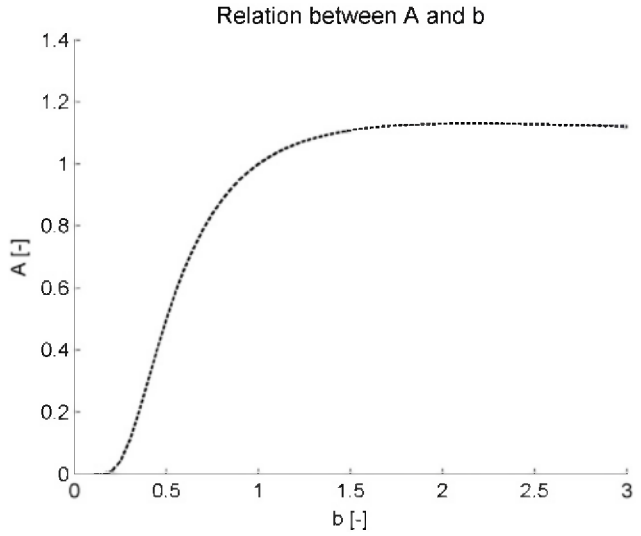

Fig. 1. Relation between A and b.

$$\begin{aligned}
\frac{N_{ow}^{Besley}}{N_w} &= 55.4 \cdot Q_*^{0.634} && \text{for } Q_* < 8 \cdot 10^{-4} \\
\frac{N_{ow}^{Besley}}{N_w} &= 2.50 \cdot Q_*^{0.199} && \text{for } 8 * 10^{-4} < Q \le 1 * 10^{-2}, \quad Q_* = q/(T_m \cdot g \cdot H_s) \\
\frac{N_{ow}^{Besley}}{N_w} &= 1 && \text{for } Q_* > 1 \cdot 10^{-2}
\end{aligned} \tag{2}$$

Other formulations for prediction of N_{ow} are presented in Pullen et al. (2007). However, these exclude the effect of the crest berm B, which is included in q in (2). Thus, since different B are evaluated in the present study, as explained later, solely the formulation in (2) is considered in the present paper.

A study on the probability distribution of individual wave overtopping volumes was carried out by Franco et al. (1994) for vertical wall breakwaters. They found that the distribution of the individual wave overtopping volumes is well fitted by a two-parameter Weibull distribution. The non-exceedance probability is thus given by (3) where $\overline{V}$ is the mean volume per individual overtopping wave. A and b are the scale factor and the shape factor, respectively. V_i is the individual wave overtopping volume.

$$F(V \ge V_i) = 1 - \exp\left[-\left(\frac{V_i/\overline{V}}{A}\right)^b\right] \tag{3}$$

By using the Weibull plotting position formula, $F(V_i) = 1 - i/(N_{ow} + 1)$, the distribution function can be expressed by (4), cf. Lykke Andersen et al. (2009).

$$\frac{V_i}{\overline{V}} = A \cdot \left[-Ln\left(\frac{i}{N_{ow}+1}\right)\right]^{1/b} = A \cdot [Ln(N_{ow}+1) - Ln(i)]^{1/b} \tag{4}$$

The maximum individual wave overtopping volume per meter width, V_{max}, can be determined by setting the rank i to 1 which leads to the expression (5). This is similar to the formulation for V_{max} presented in Pullen et al. (2007) except that they used N_{ow} instead of $N_{ow} + 1$. Lykke Andersen et al. (2009) noted that the formulation in Pullen et al. (2007) would predict $V_{max}/\overline{V} = 0$ for $N_{ow} = 1$ and thus their formulation is only valid for $N_{ow} > 5$–10. However, since many coastal protection structures are designed to obtain small N_{ow} solely the formulation in (5) is considered in this paper.

$$V_{max} = A \cdot [Ln(N_{ow}+1)]^{1/b}\, \overline{V} \tag{5}$$

The mean individual wave overtopping volume $\overline{V}$ is given by (6) which introduce a new expression for V_{max}. V_{total} is the total overtopping wave volume per meter width during a storm.

$$\begin{aligned}
\overline{V} &= \frac{V_{total}}{N_{ow}} \\
V_{max} &= \frac{A}{N_{ow}} \cdot [Ln(N_{ow}+1)]^{1/b} \cdot V_{total}
\end{aligned} \tag{6}$$

The mean value of a Weibull distribution, μ_V, given by (7), has to be equal to the mean individual wave overtopping volume and thus sets a relationship between for A and b. Γ is the mathematical gamma function.

$$\mu_V = A\Gamma\left(1 + \frac{1}{b}\right) = \overline{V} \tag{7}$$

From this, the relation between A and b is obtained given by (8) which is illustrated in Fig. 1.

$$A = \frac{1}{\Gamma\left(1 + \frac{1}{b}\right)} \tag{8}$$

b was found by Franco et al. (1994) and Van der Meer and Janssen (1994) to be approximately 0.75 for respectively caisson breakwaters and dikes in relatively deep water. The shape factor was assumed to be constant for geometrical changes of the structures. However, according to Pullen et al. (2007), b is likely to increase in shallow-water wave conditions.

Victor et al. (2012) did a more detailed analysis on the values of b, based on two-dimensional physical model tests, in which the shape factor was fitted to the distribution of measured individual wave overtopping volumes in each dataset. The aim was to improve the knowledge on the probability distribution of individual wave overtopping volumes on steep, low-crested smooth structures such as floating wave energy converters. The effect of slope angle, non-Rayleigh-distributed incident waves, relative crest freeboard, and wave steepness was evaluated. A prediction formula for b was suggested based on the trends in the findings, and was concluded to fit relatively well to the b-values obtained from the different tests, although with some scatter. The tests by Victor et al. (2012) indicated an exponential decreasing trend of the shape factor b for increasing relative crest freeboard in the range $0.1 \le R_c/H_{m0} \le 1.69$ (i.e. for relative small freeboards), where H_{m0} is the significant wave height based on frequency domain analysis and R_c is the crest height. Additionally, a linear increase in b was observed for an increasing slope angle in the range $0.36 \le \cot\alpha \le 2.75$ (i.e. for relatively steep slopes). The non-Rayleigh-distributed waves

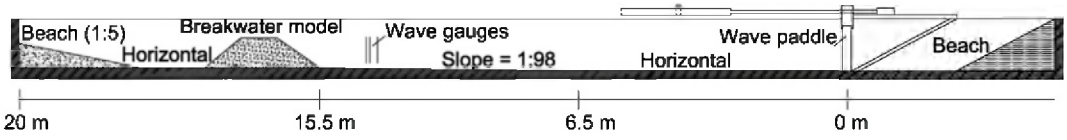

Fig. 2. Layout of model test in 2D wave flume.

Table 1
Test ranges for deep-water and shallow-water wave conditions (Nørgaard et al., 2012b).

Test series	h [m]	H_{m0} [m]	$T_{-1,0}$ [s]	H_{m0}/h [−]	A_c/H_{m0} [−]	$H_{m0}/L_{-1,0}$ [−]
Shallow-water	0.300–0.360	0.150–0.180	1.826	0.500	1.00–1.600	0.047–0.061
Deep-water	0.500–0.560	0.100	1.826	0.179–0.200	0.800–1.400	0.027–0.028

resulted in larger values of b, but within the applied range of H_{m0}/h between 0.04 and 0.38 (for steep low-crested uniform slopes) the effect of shallow-water wave conditions was concluded to be within the scatter of the empirical coefficients in the prediction formula. Finally, the influence from the wave steepness was concluded to be negligible. The prediction formula by Victor et al. (2012) is given by (9).

$$b\left(\frac{R_c}{H_{m0}}, \cot\alpha\right) = \exp\left(-2.0\frac{R_c}{H_{m0}}\right) + 0.56 + 0.15\cot\alpha \tag{9}$$

3. Physical model tests

The physical model tests used for the present analysis are further described and interpreted in Nørgaard et al. (2012a, 2012b), concerning wave loads and stability of rubble mound crown wall superstructures, respectively. The present paper will, however, solely deal with the measured wave overtopping. The tests are performed in a 25 m long and 1.5 m wide wave flume at Aalborg University, illustrated in Fig. 2. The length scale is approximately 1:30. Three resistance type wave gauges are installed near the toe of the breakwater to measure the surface elevation and to separate reflected and incident waves. The wave gauges are positioned based on suggestions by Klopman and van der Meer (1999), and the reflected and incident spectra are determined based on the approach by Mansard and Funke (1980).

3.1. Considered wave conditions

Waves are generated based on the three parameter JONSWAP spectra defined by H_{m0}, the peak frequency f_p $(=1/T_p)$, and the so-called peak enhancement factor γ. At least 1000 waves are generated in each test. The wave generation paddle is a hydraulically driven piston mode generator, and the software AwaSys (Aalborg University, 2010) is used to generate waves with simultaneously active absorption of reflected waves. Test ranges for the deep and shallow-water wave conditions are specified in Table 1, respectively. The water depth h is increased in steps in the "*deep-water case*" (resulting in changing H_{m0}/h ratios), and both h and H_{m0} are stepwise increased in the "*shallow-water case*" (the H_{m0}/h ratio is maintained). A_c is illustrated in Fig. 3.

3.2. Structure geometries

The armor layer consists of rock units with $D_{n50} = 40$ mm, and the filter layer consists of rock units with $D_{n50} = 20$ mm. The armor layer is designed to remain stable in all tests. The core consists of relative coarse material ($D_{n50} \approx 5$ mm) for both the deep and shallow-water configurations. The reason for the coarse core material is, as suggested by Burcharth et al. (1999), to compensate for the scale effects due to the non-turbulent flow in the model core material. Scale and model effects will be discussed more in details in a later section.

Different R_c/A_c ratios are tested by raising the wall height. The wave conditions in Table 1 are repeated for each modification of the structure. The ratios of the tested structure geometries are listed in Table 2. Definitions used in the table are illustrated in Fig. 3.

A photo from the shallow-water model test set-up is shown in Fig. 4. The pressure transducers and the "sliding section" in the photo are further described in Nørgaard et al. (2012a, 2012b).

3.3. Determination of wave overtopping

The set-up for determining the average overtopping rate and the individual overtopping wave volumes is illustrated in Fig. 5. The overtopping waves are directed into the box by means of a ramp, and the overtopped volumes are measured by use of a depth gauge installed inside a perforated pipe to dampen the surface elevation due to slushing in the box after an overtopping event. A pump in the overtopping box is programmed to start and stop when the water level reaches a certain predefined level. The run-time of the pump is stored in a data file and based on the pump capacity the accumulated overtopping volume is determined by compensating for the draining from the pump. The volume of the overtopping box is adjusted to each test series in order to have sufficient changes in water levels by individual wave overtopping and sufficient volume. If the overtopping box is too large compared to the wave overtopping in the specific test it is difficult to determine the individual overtopping volumes with sufficient accuracy due to too small changes in the water level in the box after an overtopping event.

An example of the processing of the overtopping signals is shown in Fig. 6. The dashed lines in Fig. 6 (*left*) illustrate pump operations. The individual overtopping volumes are identified from the cumulative overtopping volume time series. The individual volumes and the number of overtopping volumes are obtained from an algorithm, which identifies fast changes in the volume of the box. This approach is validated before the tests where specific water volumes are released and afterwards correctly detected. Moreover, the individual overtopping wave volumes and number of overtopping volumes obtained from the algorithm are compared to V_i and N_{ow} obtained by visual inspections of the accumulated overtopping wave volume time series after each test. The circles in Fig. 6 (*right*) illustrate the maximum individual wave overtopping volume in the specific example.

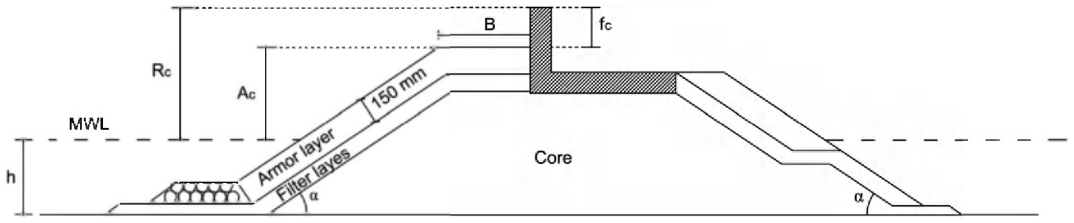

Fig. 3. Illustration of geometrical definitions (Nørgaard et al., 2012b).

Table 2
Ranges of structure dimensions for the breakwater model (Nørgaard et al., 2012b).

	R_c [m]	A_c [m]	cot(α)	B [m]	R_c/A_c [−]	A_c/B [−]
Shallow-water	0.20–0.29	0.20–0.24	1.5	0.24	1.00–1.33	0.83–1.00
Deep-water	0.1–0.19	0.1–0.14	1.5	0.17	1.00–1.70	0.59–0.82

4. Method of analysis and remaining content of paper

Initially, the wave height distributions in the deep-water and shallow-water tests are determined and compared to existing wave height distribution functions.

Secondly, the measured average wave overtopping rates q from the model tests are compared to predictions by the *CLASH Overtopping Neural Network* (van Gent et al., 2007) to evaluate whether the *Overtopping Neural Network* is capable of providing good predictions in both deep and shallow water wave conditions. This is important since predicted q are used also for prediction of N_{ow}^{Besley}, cf. (2), and thus V_{max}.

The predicted values of N_{ow}^{Besley} are then compared to the N_{ow}^{meas} determined in the model tests, and modification to the Besley formula is introduced for the shallow water conditions.

Finally, the performance of the shape factors b by Franco et al. (1994), Van der Meer and Janssen (1994), and Victor et al. (2012) is evaluated for estimation of V_{max} in deep-water and shallow-water wave conditions by comparison with V_{max} determined in the tests. A correction term is introduced to account for shallow water wave conditions.

Scale and model effects in the laboratory tests are discussed after the analysis.

5. Wave height distribution in tests

Two examples of measured deep-water and shallow-water wave height distributions are shown in Fig. 7 (*left*) and (*right*), respectively. The individual wave heights are measured at the wave gauges near the breakwater toe, c.f. Fig. 2. A Rayleigh distribution and a Battjes and Groenendijk (2000) distribution are compared to the data. The tests are divided into deep-water wave conditions, $H_{m0}/h \leq 0.2$, and shallow-water depth-limited wave conditions, $H_{m0}/h > 0.2$. As seen, the Rayleigh distribution fits well to the deep-water waves, but it is significantly overestimating the highest waves in the shallow-water wave conditions. The Battjes and Groenendijk (2000) distribution fits to the data very well in both the deep-water and shallow-water wave conditions in the example.

Fig. 4. Photo of laboratory test set-up.

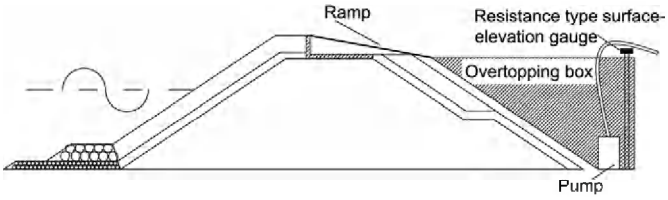

Fig. 5. Overtopping tank installed behind the breakwater.

In Fig. 8 (*left*) and (*right*), the measured and predicted values of $H_{1/10}$, based on the Rayleigh distribution and Battjes and Groenendijk (2000) distribution, respectively, are compared for all tests. $H_{1/10}$ is the average of the 1/10 highest incident waves and is evaluated since it will later be used to incorporate the effects of shallow water wave conditions in existing formulae. As seen, the Rayleigh distribution fits well to the deep-water waves but over predicts $H_{1/10}$ in shallow-water wave conditions. The Battjes and Groenendijk (2000) distribution provides very good predictions in both the deep and shallow-water wave conditions.

6. Evaluation of design tools for determination of average overtopping rate

The state of art tool *CLASH Overtopping Neural Network* (van Gent et al., 2007) is evaluated to determine its ability for prediction of q in deep and shallow-water wave conditions. The overtopping neural network is based on more than 10,000 model tests collected and performed during the EC funded CLASH project. Measured average overtopping volumes from the present tests are compared to the predicted volumes in Fig. 9. A roughness coefficient of $\gamma_f = 0.5$ is used for prediction of q as recommended in the manual. As seen, a good agreement between measured and predicted q is obtained for the evaluated deep-water and shallow-water wave conditions except for the smallest rates.

7. Evaluation of measured number of individual wave overtopping wave volumes against existing knowledge

Fig. 10 shows a comparison of the measured number of individual overtopping waves in each test with predictions given by Besley (1999) in (2). It is seen that the formula by Besley (1999) gives a relatively good estimation of N_{ow} for $H_{m0}/h \leq 0.2$, but provides an underestimation of N_{ow} for non-Rayleigh-distributed incident waves. The underestimation is due to the fact that in deep water wave conditions the individual overtopping wave volumes are characterized by a few large volumes and many smaller volumes, c.f. the Rayleigh distribution. Contrarily, the individual overtopping wave volumes in shallow water wave conditions are more uniformly distributed with many relatively large overtopping wave volumes. Thus, less overtopping waves are needed in shallow-water wave conditions to obtain the same q as in deep-water wave conditions. This leads to a higher number of individual overtopping waves in shallow-water wave conditions compared to the deep-water wave conditions.

A correction factor related to non-Rayleigh-distributed waves is thus needed to the Besley (1999) formula in order to expand the validity to non-Rayleigh-distributed waves. The correction is based on the incident wave height distribution, here characterized by the ratio $H_{m0}/H_{1/10}$. The choice of $H_{1/10}$ seems reasonable, because typically 5–10% of the waves in the design conditions give overtopping. Moreover, $H_{1/10}$ is a relatively statistically robust parameter and in the present case well predicted by the Battjes and Groenendijk (2000) wave height distribution.

As seen from Fig. 11 (*left*), the ratio between predicted and measured number of individual overtopping waves $N_{ow}^{meas}/N_{ow}^{Besley}$ increases approximately linearly with $H_{m0}/H_{1/10}$. $H_{1/10}$ in Fig. 11 is the measured values, but it could as well be predicted from the Battjes and Groenendijk (2000) distribution. By using the least-square method, a linear fit is

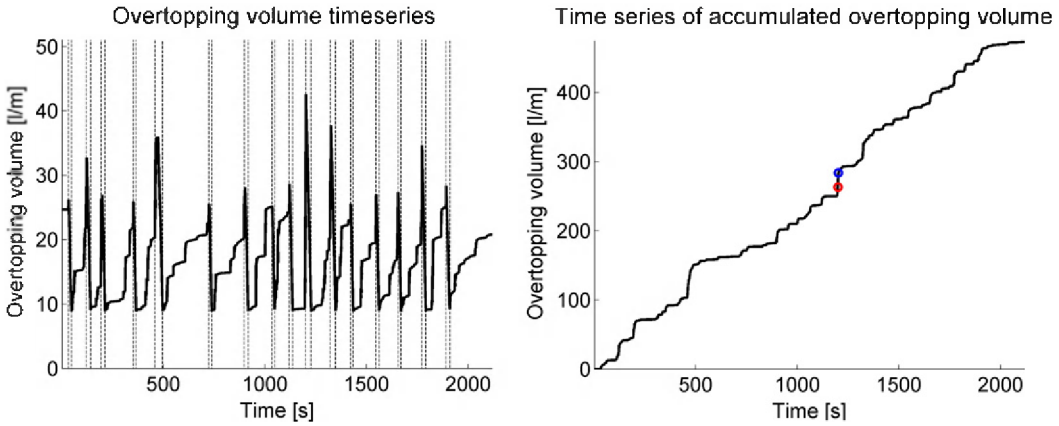

Fig. 6. (*left*) Overtopping time series in model scale measured from the depth gauge in the overtopping box. Dashed lines illustrate the operation of the pump. (*right*) Accumulated wave overtopping time series in model scale and illustration of V_{max} detection.

performed on the data in Fig. 11 (*left*) resulting in the correction factor C1($H_{m0}/H_{1/10}$), given by (10). Based on the Rayleigh distribution, the ratio $H_{m0}/H_{1/10}$ can be calculated as $H_{m0}/H_{1/10} = 0.848$ since $H_{1/3} = H_{m0} \cdot 0.927$ as proposed by Holthuijsen (2007) has been used. The linear fit is thus constrained with $N_{ow}^{meas}/N_{ow}^{Besley} = 1$, meaning that no correction is performed for perfectly Rayleigh-distributed waves. Moreover, since $N_{ow}^{meas}/N_{ow}{}^{Besley} \approx 1$ for $H_{m0}/h \leq 0.2$ C1 is solely fitted to the data for $H_{m0}/h > 0.2$.

$$N_{ow}^{mod} = N_{ow}^{Besley} \cdot C1$$
$$C1 = \begin{cases} 1 & \text{for} \quad H_{m0}/H_{1/10} \leq 0.848 \quad \text{or} \quad H_{m0}/h \leq 0.2 \\ -6.65 + \frac{H_{m0}}{H_{1/10}} \cdot 9.02 & \text{for} \quad H_{m0}/H_{1/10} > 0.848 \quad \text{and} \quad H_{m0}/h > 0.2 \end{cases} \tag{10}$$

It should be noted that the correction term C1 is only validated within the tested range: $7.3 \cdot 10^{-7} < Q_* \leq 6.19 \cdot 10^{-5}$. The correction should be smaller for higher Q_* since $N_{ow}/N_w \leq 1$.

In Fig. 11 (*right*), the modified predicted numbers of individual overtopping waves, N_{ow}^{mod}, are plotted against the measured numbers of individual overtopping waves, N_{ow}^{meas}. The performances of the original formula and the modified formula for determination of N_{ow} are evaluated based on the correlation coefficients, ρ, and the standard deviations σ. As seen, the modified N_{ow} seems to be well predicted for both incident Rayleigh and non-Rayleigh-distributed waves.

8. Individual wave overtopping volumes

The predicted maximum individual wave overtopping volume using (6), V_{max}^{pred}, based on N_{ow}^{meas}, is plotted against the measured maximum individual wave overtopping volume, V_{max}^{meas}, in Fig. 12. V_{max}^{pred} is determined using two different values of the shape factor; $b = 0.75$ in accordance with Franco et al. (1994), Van der Meer and Janssen (1994), and $b(R_c/H_{m0}, \alpha)$ by Victor et al. (2012), as presented in (9). It should be mentioned that the formulation for b by Victor et al. (2012) is not calibrated against tests on porous, rough rubble-mound slopes. However, in contrast to the shape factor by Franco et al. (1994), it includes the influence from the relative freeboard and the slope angle, and is therefore used for comparison. Moreover, as mentioned before, the shape factor by Franco et al. (1994) is based on vertical breakwaters.

As seen, V_{max}^{pred} is relatively well predicted for deep-water waves in Fig. 12 (*left*) where a slightly better performance is obtained for the shape factor presented by Victor et al. (2012). However, when evaluating the non-Rayleigh-distributed incident waves in Fig. 12 (*right*), V_{max}^{pred} is over-predicted. This indicates that a correction term for the wave height distribution in shallow water wave conditions is needed in the shape factor.

In Fig. 13 (*left*) is shown the b-factor as function of $H_{m0}/H_{1/10}$. b is determined by a least-square fit against the 30% highest individual wave overtopping volumes, $V_i > V_{30\%}$, in each test. The reason for evaluating $V_i > V_{30\%}$ is to maintain a sufficient accuracy in the determination of V_i in the model tests with the lowest amount of wave overtopping. When V_i become too small the detected overtopping wave volume is less accurate. Fig. 13 (*right*) shows the modification factor C2 fitted to the measured individual wave overtopping volumes. C2 is used to modify the formula for estimation of b by Victor et al. (2012) to include the effect of non-Rayleigh-distributed incident waves, see (11). The linear fits in Fig. 13 (*left*) and (*right*) are constrained in [x,y] = [0.848,0.75] and [x,y] = [0.848,1], respectively, meaning that no corrections are performed for perfectly Rayleigh-distributed waves. Again, since $b \approx 0.75$ and C2 ≈ 1 for

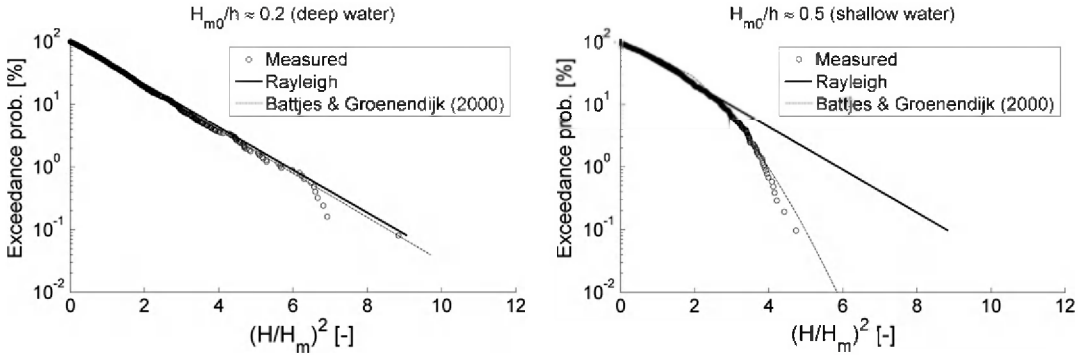

Fig. 7. Distribution of measured wave heights near the breakwater toe in (*left*) deep-water wave conditions and (*right*) shallow-water wave conditions.

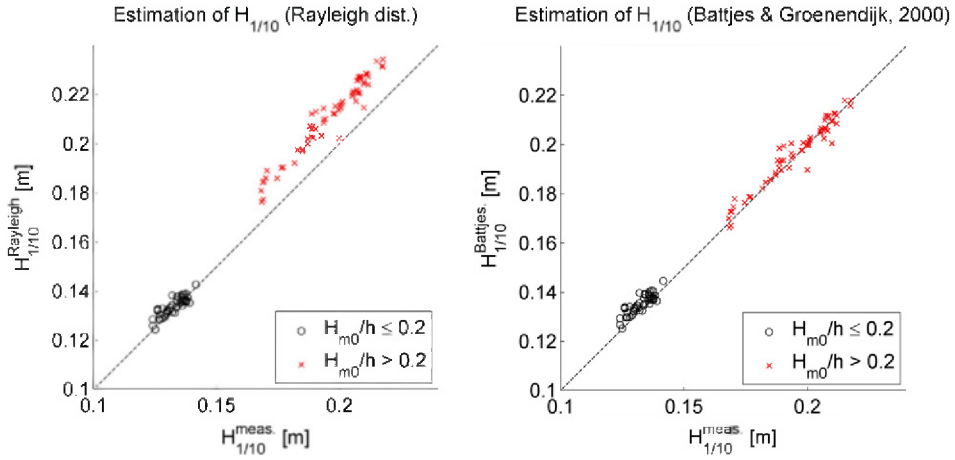

Fig. 8. Comparison of measured and predicted $H_{1/10}$ in deep and shallow-water wave conditions in model scale based on (*left*) Rayleigh distributed incident waves and (*right*) based on Battjes and Groenendijk (2000) distributed incident waves.

$H_{m0}/h \leq 0.2$ the shape factor and correction factor are solely based on the data for $H_{m0}/h > 0.2$.

$$b\left(\frac{R_c}{H_{m0}}, \cot\alpha, \frac{H_{m0}}{H_{1/10}}\right) = \left[\exp\left(-2.0\frac{R_c}{H_{m0}}\right) + 0.56 + 0.15\cot\alpha\right] \cdot C2\left(\frac{H_{m0}}{H_{1/10}}\right) \quad (11)$$

As obtained in the study by Victor et al. (2012), some scatter is present in the fitted b-factors. Most tests in shallow-water wave conditions were performed with $H_{m0}/h \approx 0.5$, which explains the fragmentation of the two data sets for the deep water and shallow-water wave conditions in Fig. 13. However, still a clear tendency is observed from the fitted line where high values of $H_{m0}/H_{1/10}$ results in high b-factors, which is also identified in the study by Victor et al. (2012) and mentioned in Pullen et al. (2007). The linear modification functions for b and C2 are given in (12) and (13), respectively. The b-factor in (12) replaces the b-factor in (11) by Victor et al. (2012), and the multiplication factor C2 in (13) is used in combination with (11).

$$b\left(\frac{H_{m0}}{H_{1/10}}\right) = \begin{cases} 0.75 & \text{for } H_{m0}/H_{1/10} \leq 0.848 \text{ or } H_{m0}/h \leq 0.2 \\ -6.1 + \frac{H_{m0}}{H_{1/10}} \cdot 8.08 & \text{for } H_{m0}/H_{1/10} > 0.848 \text{ and } H_{m0}/h > 0.2 \end{cases} \quad (12)$$

$$C2\left(\frac{H_{m0}}{H_{1/10}}\right) = \begin{cases} 1 & \text{for } H_{m0}/H_{1/10} \leq 0.848 \text{ or } H_{m0}/h \leq 0.2 \\ -10.8 + \frac{H_{m0}}{H_{1/10}} \cdot 13.9 & \text{for } H_{m0}/H_{1/10} > 0.848 \text{ and } H_{m0}/h > 0.2 \end{cases} \quad (13)$$

The modified predicted maximum individual wave overtopping volumes are plotted against the measured maximum individual wave overtopping volumes in Fig. 14, using b in accordance with (12) and C2 in accordance with (13). As seen, a relatively good agreement is obtained between measured and predicted maximum overtopping volumes for both modified shape factors. However, the shape factor by Victor et al. (2012) modified using (13) is expected to provide better predictions in case of low R_c/H_{m0}-ratios and for

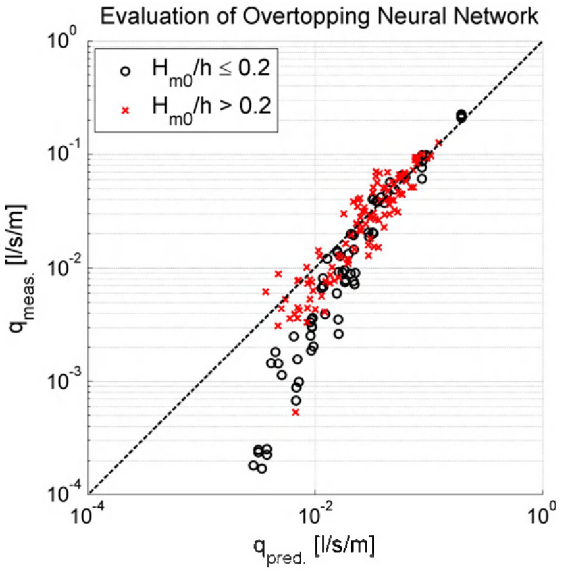

Fig. 9. Comparison of measured average overtopping rates in model scale with predictions from the "Overtopping Neural Network" in non-Rayleigh and Rayleigh-distributed waves.

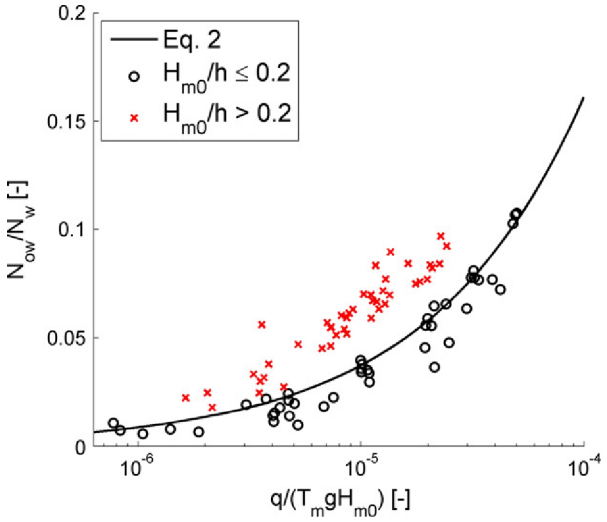

Fig. 10. Evaluation of measured N_{ow} against the formula by Besley (1999).

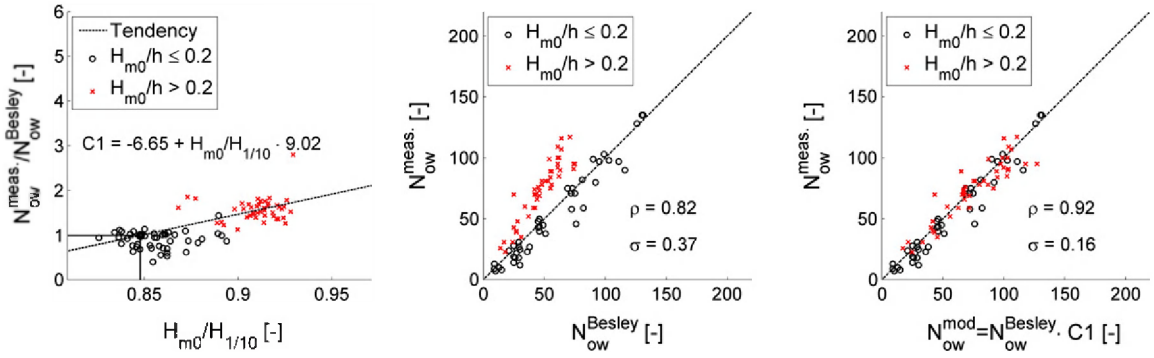

Fig. 11. (*left*) Influence from $H_{m0}/H_{1/10}$ on N_{ow}. (*middle*) Correlation between measured and predicted N_{ow} without introducing the effects of depth limited wave conditions. (*right*) Evaluation of modification factor for including the effect on non-Rayleigh-distributed incident waves in estimation of N_{ow}.

front slopes which significantly differ from the evaluated slope of $\cot(\alpha) = 1.5$.

Evaluated ranges for q in Fig. 9, the modified N_{ow} in Fig. 11, and the modified V_{max} in Fig. 14, are summarized in Table 3.

It should be kept in mind that no variation is performed on the slope angle in the model tests and that the breakwater profile is a traditional high crested profile with a roughness of $\gamma_f \approx 0.5$. The effect of varying slope angles is, however, included in the prediction formula for b by Victor et al. (2012), $0.36 \le \cot\alpha \le 2.75$.

9. Scale and model effects in model tests

Briganti et al. (2005) described the full-scale measurements of wave overtopping at the Italian Rome yacht harbor breakwater in Ostia, located in depth-limited wave conditions. They highlighted the several non-conservative scale and model effects related to wave overtopping in small-scale. Among others, they noted the expected scale effects related to heavy wave breaking in small scale and the model effects of neglected perpendicular winds in small scale, which for the considered structure in full-scale increased the average overtopping rate by a factor 5 for an increase of a factor 2 in wind speed. Only little effect from cross wind was observed.

De Rouck et al. (2007) compared the prototype measurements from the Zeebrugge rubble mound breakwater with model test data in 2-D and 3-D. They stressed the needs for accurate modeling of the permeability of armor and core material since this was seen to have a high influence on especially the run-up level. To separate scale effects from wind effects and other uncertainties regarding prototype conditions Lykke Andersen et al. (2011) carried out comparative tests in large and small scale and identified a significant scale effect on mean overtopping discharges on rubble mounds.

The influence from scale effects on N_{ow} and V_{max} has not been investigated in details. However, Lykke Andersen et al. (2009) indicated that the scale effects on these parameters are not significant.

10. Conclusions

Individual wave overtopping volumes are measured in physical model testing of a rubble mound breakwater with a crown wall. The measured average overtopping rates from the present model tests are compared to predicted rates from the Overtopping Neural Network (van Gent et al., 2007) where a relatively good agreement is found for both deep-water and shallow-water wave conditions.

Existing state of the art tools for estimation of maximum individual wave overtopping volumes are seen to perform very well in deep-water wave conditions. However, in shallow-water wave conditions, the formula by Besley (1999) is seen to under predict the number of individual overtopping waves. This is due to the fact that individual wave overtopping volumes in shallow-water wave conditions are more evenly distributed compared to deep-water waves. Thus, a correction factor is introduced, based on the incident wave height distribution, described by the ratio; $H_{m0}/H_{1/10}$.

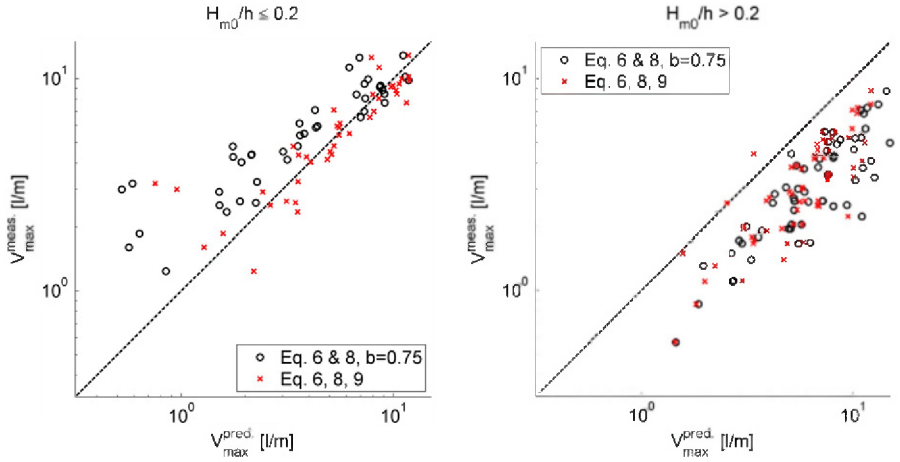

Fig. 12. Correlation between measured and predicted V_{max} in model scale in (*left*) deep-water wave conditions and (*right*) shallow-water wave conditions.

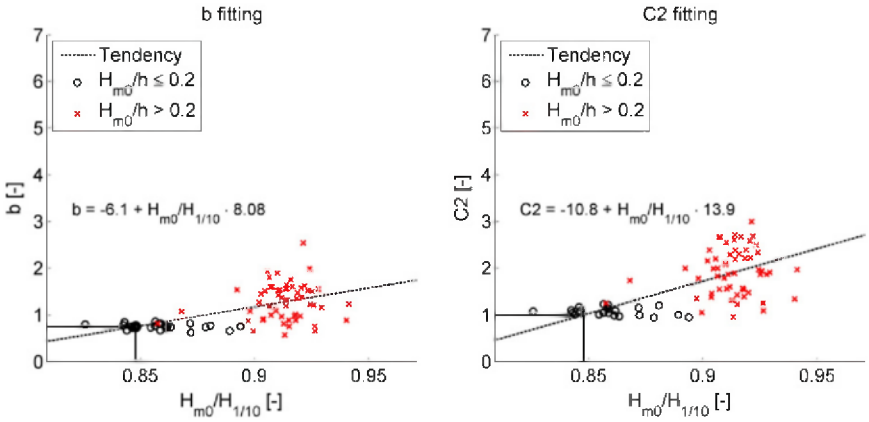

Fig. 13. Influence from non-Rayleigh-distributed waves on (*left*) b and (*right*) C2 ($V_i > V_{30\%}$).

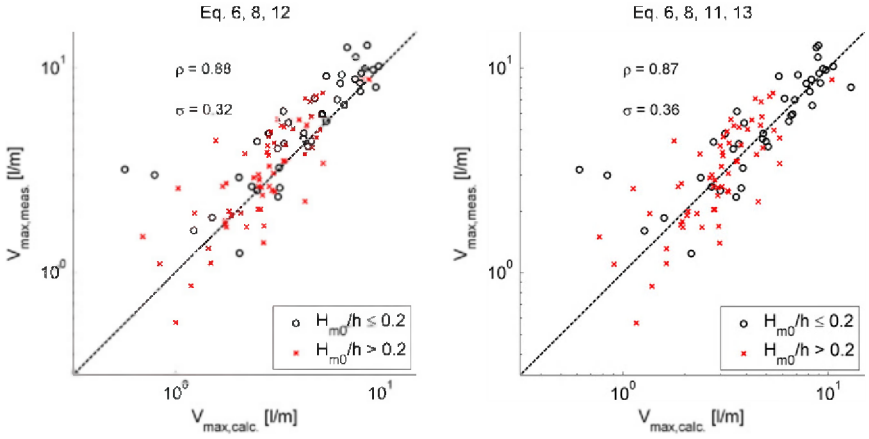

Fig. 14. Evaluation of predicted maximum individual wave overtopping volumes in model scale with (*left*) V_{max} predicted using (6) and modified b in accordance with (12) and (*right*) V_{max} predicted using (6) and modified b in accordance with (11) and (13).

The suggested shape factors by Franco et al. (1994), Van der Meer and Janssen (1994), and Victor et al. (2012) in the two-parameter Weibull distribution used for the estimation of individual wave overtopping volumes are seen to insufficiently describe the distribution of individual wave overtopping wave volumes in depth-limited waves. The existing formulae significantly over-predict the largest individual wave overtopping volumes. Thus, correction terms are suggested based on the $H_{m0}/H_{1/10}$-ratio.

Acknowledgments

The support of the European Commission through FP7.2009-1, Contract 244104 — THESEUS ("Innovative technologies for safer European coasts in a changing climate"), is gratefully acknowledged.

Table 3
Investigated parameter ranges in modified design formulae for V_{max}.

Parameters	Ranges
H_{m0}/h	0.19–0.55
R_c/H_{m0}	0.9–2.0
ξ_m	3.3–4.6
N_{ow}/N_w	0.006–0.12
$q/(T_m g H_s)$	$7.729 \cdot 10^{-7}$–$6.19 \cdot 10^{-5}$

References

Aalborg University, 2010. AwaSys webpage. http://hydrosoft.civil.aau.dk/AwaSys.htm (Department of Civil Engineering, Aalborg University).
Battjes, J.A., Groenendijk, H.W., 2000. Wave height distributions on shallow foreshores. Coast. Eng. 40, 161–182.
Besley, P., 1999. Wave overtopping of seawalls. Design and Assessment Manual. R&D Technical Report W178. HR Wallingford. ISBN: 1 85705 069 X.
Briganti, R., Bellotti, G., Franco, L., De Rouck, J., Geeraerts, J., 2005. Field measurements of wave overtopping at the rubble mound breakwater of Rome–Ostia yacht harbour. Coast. Eng. (ISSN: 0378-3839) 52 (12), 1155–1174 (December).
Burcharth, H.F., Liu, Z., Troch, P., 1999. Scaling of core material in rubble mound breakwater model tests. Proc. of the Fifth International Conference on Coastal and Port Engineering in Developing Countries, Cape Town, South Africa, pp. 1518–1528.
De Rouck, J., Van de Walle, B., Troch, P., van de Meer, J., Van Damme, L., Medina, J.R., Willems, M., Frigaard, P., 2007. Wave run-up on the Zeebrugge Rubble Mound Breakwater: full-scale measurement results versus laboratory results. J. Coast. Res. 23 (3), 584–591. http://dx.doi.org/10.2112/04-0157A.1.
Franco, L., de Gerloni, M., van der Meer, J.W., 1994. Wave overtopping on vertical and composite breakwaters. Proc. 24th International Conference on Coastal Engineering. ASCE, New York, pp. 1030–1044.
Holthuijsen, L.H., 2007. Waves in Oceanic and Coastal Waters. Cambridge University Press.
Klopman, G., van der Meer, J.W., 1999. Random wave measurements in front of reflective structures. J. Waterw. Port Coast. Ocean Eng. ASCE 125 (1), 39–45.
Lykke Andersen, T., Burcharth, H.F., Gironella, X., 2011. Comparison of new large and small scale overtopping tests for rubble mound breakwaters. Coast. Eng. (ISSN: 0378-3839) 58 (4), 351–373. http://dx.doi.org/10.1016/j.coastaleng.2010.12.004.

Lykke Andersen, T., Burcharth, H.F., Gironella, F.X., 2009. Single wave overtopping volumes and their travel distance for rubble mound breakwaters. Coastal Structures 2007: Proceedings of the 5th International Conference, Venice, Italy, 2–4 July 2007. World Scientific Publishing Co Pte Ltd., Venice, Italy, pp. 1241–1252.

Mansard, E.D., Funke, E., 1980. The measurement of incident and reflected spectra using a least-square method. Proceedings of the 17th International Conference on Coastal Engineering, vol. 2. ASCE, pp. 154–172.

Nørgaard, J.Q.H., Andersen, T.L., Burcharth, H.F., 2012a. Wave loads on crown walls of rubble mound breakwaters in deep and shallow-water wave conditions. Coast. Eng. (ISSN: 0378-3839) 80, 137–147. http://dx.doi.org/10.1016/j.coastaleng.2013.06.003 (October 2013).

Nørgaard, J.Q.H., Andersen, L.V., Andersen, T.L., Burcharth, H.F., 2012b. Displacement of monolithic rubble-mound breakwater crown-walls. 33rd International Conference on Coastal Engineering ICCE 2012, Santander, Spain.

Pullen, T., Allsop, W., Bruce, T., Kortenhaus, A., Schuttrumpf, H., van der Meer, J., 2007. Wave overtopping of sea defenses and related structure: assessment manual. www.overtopping-manual.com.

Van der Meer, J.W., Janssen, J.P.F.M., 1994. Wave Run-up and Wave Overtopping at Dikes and Revetments. Delft Hydraulics.

Van Gent, M.R.A., 2001. Wave Runup on Dikes with Shallow Foreshores. J. Waterw. Port Coast. Ocean Eng. 127 (5), 254–262.

Van Gent, M.R.A., van den Boogaard, H.F.P., Pozueta, B., Medina, J.R., 2007. Neural network modelling of wave overtopping at coastal structures. Coast. Eng. 54 (8), 586–593 (August 2007).

Victor, L., van der Meer, J.W., Troch, P., 2012. Probability distribution of individual wave overtopping volumes for smooth impermeable steep slopes with low crest freeboards. Coast. Eng. (ISSN: 0378-3839) 64, 87–101. http://dx.doi.org/10.1016/j.coastaleng.2012.01.003 (June 2012).